# Economic Efficiency of a Renewable Energy Independent Microgrid with Energy Storage by a Sodium–Sulfur Battery or Organic Chemical Hydride

Shin'ya Obara [1)], Yuta Morizane[2)], Jorge Morel [3)]

[1), 2), 3)]Kitami Institute of Technology, Power Engineering Lab., Dep. of Electrical and Electronic Engineering, Koen-cho 165, Kitami, Hokkaido 090-8507, Japan

[1)] obara@mail.kitami-it.ac.jp, phone/FAX +81-157-26-9262

## Abstract

The present study uses numerical analysis to investigate the operating methods and costs of an independent microgrid incorporating a sodium–sulfur (NAS) battery or an energy storage system using organic hydrides. Details relating to the operation of the system and its installed capacity and cost were clarified, assuming the introduction of an independent microgrid in Kitami City, a cold region in Japan. Analysis results indicate that energy storage technology using the organic hydride system is economically inferior to the NAS battery owing to large losses associated with the water electrolyzer and dehydration reactor. Therefore, for the widespread use of the organic hydride system, it is necessary to improve the efficiency of these components.

***Keywords***: local energy, organic chemical hydride, NAS battery, microgrid, energy storage, numerical simulation

## 1. Introduction

It is necessary to control unpredictable fluctuations of renewable energy to allow the development of an independent microgrid utilizing renewable energy. Introduction of a battery, which would allow high-speed control of output, is effective in this regard. In the present study, two means of controlling power fluctuations are investigated: a sodium–sulfur (NAS) battery and energy storage by a hydrogen medium incorporating the organic chemical hydride methylcyclohexane, hereafter referred to as OCHM. NAS batteries are already produced commercially and have been proposed for controlling fluctuations of large-scale renewable energy [1, 2]. Moreover, NAS batteries have been investigated extensively to assess their possible introduction to power networks [3-5]. The OCHM technology investigated here obtains hydrogen from water electrolysis, providing electric power from renewable energy, and produces methylcyclohexane through a hydrogenation reaction of this hydrogen with toluene. Because abundant hydrogen is included, the energy density of methylcyclohexane is high. Furthermore, because methylcyclohexane is a liquid, its performance in terms of conveyance and storage is excellent. Hydrogen supplied to a fuel cell or engine generator can be obtained by dehydration of methylcyclohexane, and renewable energy generated by the OCHM does not require power transmission lines for transport by land [6-8]. Moreover, although the energy density of the

OCHM is about seven times that of NAS batteries, the economic advantages of the OCHM are offset by transport costs and losses of energy from the water electrolyzer, hydrogenation reactor, and dehydration reactor. Furthermore, although direct current power can be obtained directly from NAS batteries, power generation systems must be installed to convert hydrogen obtained by dehydration of methylcyclohexane into power. Therefore, the economic advantages of addressing power fluctuations using the OCHM in an independent microgrid remain unclear.

Therefore, this study aims to clarify the equipment capacity, operating methods, and costs of an independent microgrid incorporating renewable energy and energy storage by NAS batteries or the OCHM. To this end, citywide residential energy supply is investigated for Kitami City, Japan by assuming the installation of an independent microgrid comprising a large-scale solar power system and a wind farm. The operating method of the microgrid is determined by analyzing the balance between supply and demand and energy storage such that the annual energy balance of the entire city may be satisfied. Based on the results of this analysis, the capacities, operating methods, and costs of the large-scale solar power system, wind farm, NAS battery, OCHM system, and other auxiliary equipment are clarified and compared in economic terms.

## 2. Proposed System

### 2.1 Independent Microgrid

In the present study, renewable energy equipment, an electrical power grid, energy storage equipment, and users are assumed to be located within approximately 100 km of a microgrid. For example, it is proposed that the wind farm must be installed in a coastal area, where wind speeds are high, and the large-scale solar power system must be installed in a suburb that receives sufficient solar radiation. Power fluctuations of the proposed microgrid are controlled by the introduction of a NAS battery or an energy storage system incorporating the OCHM. Heat for space heating and hot water can be generated by supplying a hot antifreeze solution from multiple heat pumps.

Table 1 presents the characteristics of NAS batteries and OCHM systems reported in previous studies; the information is obtained from NGK Insulators Ltd. [9] and examination of existing systems [10], respectively. Although the theoretical energy density of a NAS battery is greater than that of an OCHM, the actual operational energy density of an OCHM is about seven times that of a NAS battery. Moreover, the charge and discharge efficiencies of an OCHM and NAS battery are 50% and 75%, respectively. However, while the charge and discharge efficiencies of a NAS battery are based on the charge and discharge (AC output) of electric power, those of the OCHM depend on energy storage and release based on the heating value of hydrogen. Although specific details of the design life of the OCHM are unknown, it is expected that periodic replacement of the catalyst layer will be required because the dehydration reactor will be maintained at temperatures of 300°C or more. The facilities cost for the OCHM is much higher than that for NAS batteries. However, since the operating costs of the OCHM are very small compared to those of NAS batteries, the economic efficiency of the OCHM may become advantageous for large outputs and long operating times.

Seasonal energy variations are possible with both NAS batteries and the OCHM. Therefore, the installed capacity is determined on the basis of annual energy supply and demand balances.

Accordingly, surplus renewable energy generated in the summer season, when little heat is required, is stored by NAS batteries or by hydrogenation of toluene (liquid methylcyclohexane). Then, the energy stored in summer is supplied to the demand side in winter through discharge of the NAS batteries or dehydration of methylcyclohexane in order to meet the higher heat demand. The amount of renewable energy supplied can be controlled by introducing seasonal energy variations into the microgrid.

2.2 Independent Microgrid with NAS Batteries

Figure 1 (a) illustrates the proposed independent microgrid system for the NAS battery. Electric power supplied to a power transmission line from renewable energy sources (a large-scale solar power system and a wind farm) is 6.6 kV for a three-phase circuit three-wire alternating current (AC) system. The electric power supplied to the demand side is converted into 200 V AC by a transformer that is part of the power distribution network. Voltage fluctuations of ±20% can be compensated by the NAS battery via charge and discharge. The rated temperature of the NAS battery is 300°C and the battery is heated by an electric heater. Electric power generated by renewable methods is distributed to the system and supplied to the NAS battery through DC/AC conversion, system supplied to heat pump, and system supplied to the power distribution network. The NAS battery plays two roles: stabilization of the supply and demand balance and introduction of seasonal energy variations. The microgrid illustrated in Fig. 1 (a) is referred to as the NAS battery type.

2.3 Independent Microgrid with Energy Storage by an Organic Hydride

When incorporating energy storage by OCHM into a microgrid, the operations involved are similar to those for a storage battery (Fig. 1 (b)), and the OCHM is transported instead of power being transmitted through power lines (Fig. 1 (c)). When there is a deficit in the supply of renewable energy, as shown in Fig. 1 (b), hydrogen obtained by dehydration of methylcyclohexane is supplied to a power generator. However, the stored methylcyclohexane is supplied to a generator installed near the power distribution network through land transportation, e.g., by a pipeline, as shown in Fig. 1 (c). In the case of the system illustrated in Fig. 1 (c), existing infrastructure (such as conventional tankers and gas stations) can be used. In the present study, the systems illustrated in Figs. 1 (b) and (c) are referred to as OCHM-A and OCHM-B systems, respectively.

3. System Components

3.1 Renewable Energy

3.1.1 Wind Farm

3.1.1.1 Wind generator system used for the NAS battery system

The wind generator system can be classified as a direct drive duplex feeding induction generator (DFIG), and DFIGs have been adopted extensively for use as power generators in combination with large adjustable-speed wind turbines. All wind generator systems included in the wind farm installed in the NAS battery system are assumed to be of the DFIG type. Figure 2 (a) is a block diagram illustrating the independent microgrid of the NAS battery system. The DFIG wind generator is shown in the upper part of Fig. 2 (a) and a photovoltaic is illustrated in the lower part. The wind farm and

large-scale solar power system included in the NAS battery microgrid require the installation of two or more sets of the wind generator and photovoltaic systems illustrated in Fig. 2 (a).

In the DFIG type, the primary stator coil is connected to the electric power system, and AC with a frequency determined by the difference between the rotational frequency of the rotor and the system frequency is supplied to the secondary coil of the rotor, which is connected to the wind turbine. By magnetizing this secondary coil, output generated with the system frequency can be obtained at the output of the primary stator coil. The mechanical and electrical rotor frequencies are separated, and the rotor frequency can be synchronized with the system frequency. DFIG wind generator systems have high power generation efficiency and low facilities cost because the inverters have a small capacity. The effective power output from the inverter $P_{GW3}$ is defined by Eq. (1). Here, $s$ is the sliding variable calculated using Eq. (2), $n_0$ is synchronous speed, and $n$ is the engine speed of the power generator. The effective power supplied to the demand side $P_{GW}$ is derived using Eq. (3). Moreover, the generated electric power is supplied to the power distribution network, NAS battery, and heat pump via the bus line SC_wp in Fig. 2 (a).

$$P_{GW3} = -s \cdot P_{GW1} \tag{1}$$

$$s = (n_0 - n)/n_0 \tag{2}$$

$$P_{GW} = P_{GW1} + P_{GW3} = (1 - s) \cdot P_{GW1} \tag{3}$$

3.1.1.2 Wind generator system used for the OCHM system

In the wind farm introduced into the OCHM microgrid illustrated in Figs. 1 (b) and (c), wind power is generated by a permanent magnet type synchronous generator. The OCHM system with a wind farm and large-scale solar power system supplies electric power to the power distribution network, water electrolyzer, heat pump, and hydrogen compressor. Figure 2 (b) is a block diagram illustrating the microgrid of the OCHM type. Power transmitted to reduction gears from the turbine of the wind generator system is given to the synchronous generator, as shown in the upper part of the figure, and the output of the power generator is supplied to bus line SC_wp through AC/DC, DC/AC, and system interconnection equipment. Electric power is supplied to a distribution network, water electrolyzer, heat pump, and hydrogen compressor from bus line SC_wp in the OCHM-A system, whereas electric power is supplied to a water electrolyzer and hydrogen compressor in the OCHM-B system. The measured value of the electric power generated from wind power in Fig. 2 (b) sends from Wattmeter (1) to Controller (1), outputting a high-speed command signal from Controller (1) to the AC/DC converter next to the water electrolyzer, which corresponds to electric power generation. The current used for cold water electrolysis corresponds to the difference between the electric power generated and the load (i.e., the total power consumed owing to the electricity demands of the hydrogen compressor and heat pump). Although the output of wind power generation is sharply changed within several ten seconds, it has been confirmed previously [11] that hydrogen production by water electrolysis can cope with such fluctuations.

3.1.2 Large-scale Solar Power System

The use of photovoltaics in a large-scale solar power system requires the same equipment as that used for the NAS battery and OCHM systems, assuming that bifacial photovoltaics are used [12]. The electric power output from the solar module is supplied to bus line SC_pv through a snubber circuit (protection circuit), DC/DC converter, inverter, three-phase AC harmonic filter, and system interconnection equipment. Electric power is distributed to the NAS battery, power distribution network, and heat pump from the bus line SC_pv in the NAS battery system, while electric power is distributed to a power distribution network, water electrolyzer, hydrogen compressor, and heat pump from bus line SC_pv in the OCHM-A system. Electric power is supplied to the water electrolyzer and hydrogen compressor from bus line SC_pv in the OCHM-B system.

3.2 Fuel Cell

The lower part of Fig. 2 (b) is a block diagram of a fuel cell introduced into the microgrid of the OCHM-A and OCHM-B systems. The fuel cell is assumed to be a solid oxide fuel cell (SOFC) and the power output is controlled by adjusting the fuel supply using an electric energy signal transmitted by Controller (2) via bus line SC_fc. Furthermore, to interconnect the fuel cell with the electric power system, it is necessary to synchronize the supply capability with the electric power system. Therefore, the synchronization of the fuel cell and other electric power systems is adjusted by measuring the voltage of bus line SC_fc and outputting a feedback signal to the inverter from the PWM generator.

3.3 NAS battery

Figure 3 (a) outlines the NAS battery introduced into the proposed system. The NAS battery must maintain all active materials in a molten state, and the ionic conduction properties of beta alumina are enhanced at high temperatures (300–350°C). Equations (4) and (5) describe the reactions of the NAS battery. Although the anode is a two-component region, with neutral sulfur and $Na_2S_5$ in the initial discharge (i.e., the last stage of charge), it has only one component ($Na_2S_x$; $x<5$) at advanced stages of discharge.

$$2Na + xS \rightleftharpoons Na_2S_5 + (x-5)S, \text{ for } x>5 \quad (4)$$

$$2Na + xS \rightleftharpoons Na_2S_x, \text{ for } x<5 \quad (5)$$

The theoretical specific energy of sulfur $Na_2S_x$ is 755 Wh/kg, while the total theoretical specific energy is 784 Wh/kg or 1005 Wh/l. Because energy consumption by auxiliary equipment, loss of reaction heat, and overvoltage occur, the actual specific energy is only 100–160 Wh/kg. As the characteristics of the NAS battery are strongly dependent on battery temperature, a complete analysis of transient characteristics must consider the effects of battery temperature. Therefore, the amount of heat radiation emitted by the battery is calculated, as shown in Fig. 3 (b), from the difference between the outside air temperature and the reference temperature. Then, the operating temperature of the battery is calculated from its heat capacity. This operating temperature is controlled as illustrated in

the block diagram of Fig. 3 (c) in order to modify the difference between the working temperature and battery temperature. Moreover, the charge and discharge efficiencies and energy density, which are affected by changes in battery temperature, are derived from the relationship between battery temperature and the battery temperature characteristics described above.

3.4 Energy Storage in a Hydrogen Medium Using an Organic Chemical Hydride

3.4.1 Water Electrolysis

Equation (6) describes the water electrolysis reaction; the standard enthalpy of water formation at 1 atm and 25°C is $\Delta H^{\circ} = -285.8$ kJ/mol. Typically, the energy efficiency of a water electrolyzer by quality of alkaline type water electrolysis is 70–75%. The electric power supplied to the water electrolyzer and the quantity of hydrogen produced depend on the standard enthalpy of water formation and the energy efficiency of the water electrolyzer.

$$H_2O \rightarrow H_2 + 1/2O_2 - 285.8\,\mathrm{kJ/mol} \tag{6}$$

3.4.2 Hydrogenation and Dehydration Reactions

Equation (7) describes the hydrogenation of toluene ($C_7H_8$) and Eq. (8) describes the dehydration of methylcyclohexane ($C_7H_{14}$). For optimum reaction temperatures and pressures, the ratios of chemical reaction of the hydrogenation and dehydration reactions are 100% and 99%, respectively. Catalysts such as Ru-$CeO_2$ are used for the hydrogenation reaction under conditions of 1 MPa and 70°C. On the other hand, catalysts such as those containing Pt are used for the dehydration reaction under conditions of 1.1 MPa and 300–350°C. Because the dehydration reaction requires heat supply, its energy efficiency is typically around 85%.

$$C_7H_8 + 3H_2 \rightarrow C_7H_{14} + 204.8\,\mathrm{kJ/mol} \tag{7}$$

$$C_7H_{14} \rightarrow C_7H_8 + 3H_2 - 204.8\,\mathrm{kJ/mol} \tag{8}$$

3.4.3 Water Electrolyzer and Hydrogenation Reactor

Figure 4 presents a block diagram of the hydrogenation reactor adopted in this study. Hydrogen is produced by supplying the water electrolyzer with electric power derived from renewable energy. The resulting hydrogen is further pressurized to 1.0 MPa by a compressor. The work of the compressor is assumed to be the work required for the compression of an ideal gas and is calculated as in Eq. (9). $\varphi_c$ in this equation represents the overall efficiency of the compressor and incorporates several components: power consumption of the inverter control equipment and electric motor, transfer loss of power, loss through air leaks, insufficient cooling, and other mechanical loss. Moreover, $L_{c,H_2,t}$, $U_{\infty}$, and $C$ represent the work of the compressor, flow of hydrogen, and pressure, respectively.

$$L_{c,H_2,t} = C_\infty \cdot U_{\infty,t} \cdot \ln\left(C_{Comp,H_2} / C_\infty\right) / \varphi_c \tag{9}$$

The performance of the water electrolyzer and hydrogenation reactor depends on temperature. Therefore, the amount of heat radiated from these components is calculated as the difference between the outside air temperature and the reference temperature, as shown in the block diagram of Fig. 4 (a). Furthermore, the present operating temperature is calculated from the heat capacity of the equipment, and the reaction temperature is controlled by the difference between the operating temperature and working temperature, as shown in the block diagram of Fig. 4 (b). The reaction efficiency, which is based on the equipment temperature, is obtained with reference to the relationships between the reaction temperature and output characteristics of each component of the system ( $K_{c,t}$ in Fig. 4 (b))

3.4.4 Dehydration Reaction Equipment

Figure 5 presents a block diagram of a reactor incorporating the dehydration reaction described by Eq. (8). The rate of the dehydration reaction is dependent on temperature. Therefore, reaction temperature must be considered when assessing the heat capacity of the equipment shown in Fig. 5 (b), and the amount of heat radiated owing to the difference in temperature between the outside air and the reactor must be calculated. Furthermore, the rate of dehydration (for a given sampling time) is calculated according to the block diagram of Fig. 5 (a).

4. Control Method

4.1 Microgrid of the NAS Battery Type

The control method for the microgrid of the NAS battery type is illustrated in Figs. 1 (a) and 2 (a) and is as described below. Electric power from the DFIG wind farm ( $P_{GW}$ in Fig. 2 (a)) is supplied to bus line SC_wp. On the other hand, electric power from a large-scale solar power system ( $P_{GS}$ in Fig. 2 (a)) is supplied to bus line SC_pv and connects electric power of SC_pv and SC_wp on an electric power system. The electric power of SC_wp and SC_pv synchronizes with the output power of the base power generator of Fig. 2 (a) through transmission of a control signal to the inverter control equipment of the wind farm and solar power system. Furthermore, the maximum output point control is introduced into the photovoltaics and the operating point of modular current and voltage is controlled by a common solar cell at a maximum output point.

Charge and discharge of the NAS battery are set with reference to the frequency measured by wattmeters installed at the wind farm and solar power system and are controlled by commands issued to the AC/DC converter of the NAS battery by Controller (2) in Fig. 2 (a). Because surplus electricity is generated when the measured frequency exceeds the rated value, Controller (2) commands charge operation the AC/DC converter of NAS battery. On the other hand, because the supply of electric power is insufficient when the measured frequency is less than the rated value, Controller (2) commands discharge operation the AC/DC converter of NAS battery.

4.2 Microgrid of the OCHM Type

The control method for the microgrid with energy storage by the OCHM is illustrated in Figs. 1 (b) and (c). When managing the OCHM in addition to the NAS battery (OCHM-A, Fig. 1 (b)), power generated by renewable means is supplied to an electrical power grid through a power transmission line and the surplus power is supplied to the water electrolyzer. The power supply and demand balance for the wind farm and solar power system can be determined by Controller (1) measuring the frequency at each wattmeter, as illustrated in the upper part of Fig. 2 (b). The shortfalls and excesses of electric power are assessed on the basis of this frequency, and Controller (1) commands hydrogen production the AC/DC converter of water electrolyzer when surplus power is supplied. On the other hand, when the power supply is insufficient, the controller outputs a command to increase production of electricity by the SOFC, as shown in the lower part of Fig. 2 (b).

Power generated by the wind farm and large-scale solar power system is supplied to the water electrolyzer, power distribution grid, hydrogen compressor, and heat pump in the OCHM-A microgrid. Moreover, bus lines SC_wp, SC_pv, and SC_fc in Fig. 2 (b) are interconnected with the electric power system. However, although the power generated by the wind farm and solar power system in the OCHM-B system is supplied to the water electrolyzer and hydrogen compressor through bus lines SC_wp and SC_pv, bus line SC_fc operates independent of SC_wp and SC_pv.

Hydrogen generated by the water electrolyzer is supplied to the hydrogenation reactor, which is filled with toluene, and methylcyclohexane is generated in the OCHM system. This methylcyclohexane is supplied to a catalyst layer in the dehydration reactor and desorption of hydrogen is promoted by the application of heat. The inverter is controlled by the fuel cell system illustrated in the lower part of Fig. 2 (b), such that the frequencies of the electric power system and the power $P_{GF}$ become synchronized. Moreover, shortfalls and excesses of electricity are assessed by Controller (2) based on the frequency of the electric power system. The supply of $H_2$ to the fuel cell is changed accordingly, allowing the generation of electricity power to be adjusted. Furthermore, the power of the fuel cell is stabilized by a flow rate regulator.

5. Analysis Example

5.1 Proposed System

A microgrid is installed at Kitami City in Hokkaido, Japan for this analysis. Kitami is the largest city in the Sea of Okhotsk area of Hokkaido and has a population of about 125,000 in around 61,214 residences. The installation of wind power generation equipment and a large-scale solar power system (in the coastal area and inland, respectively) is planned for Kitami City. The city experiences a maximum air temperature of 35°C in summer and a minimum temperature of −20°C in winter; and the temperature range is larger inland than at the coast. The annual mean air temperature in Kitami is about 6°C, and the city experiences the lowest winter temperatures among all urban areas in Japan. However, little rainfall or snowfall occurs in the city. Figure 6 outlines the microgrid installed at Kitami. The detailed climate condition is released by the Japanese Meteorological Agency [13].

The NAS battery is installed at the energy supply base in the NAS battery system. Moreover, a water electrolyzer, hydrogenation reactor, dehydration reactor, and fuel cell are installed at the energy supply

base in the OCHM-A system. The energy supply and generation bases are connected by a power transmission line in both systems. Moreover, electric power generated by renewable methods is supplied to the energy generation base (Fig. 6), and electricity is transmitted to the energy supply base through the power transmission line. On the other hand, in the OCHM-B system, hydrogen produced at the energy generation base is incorporated into methylcyclohexane in the hydrogenation reactor. Then, methylcyclohexane is transported to the energy supply base by land. The dehydration reactor and fuel cell are installed at the energy supply base, from which electric power is supplied to the distribution network. No transmission line is installed between the energy generation and supply bases in the OCHM-B system.

5.2 Performance and Cost of Equipment

The performance of the equipment constituting the proposed system is shown in Table 2. Figure 7 shows the characteristics of a heat pump for cold regions that uses a $CO_2$ coolant that is currently commercially available. These characteristics were chosen because the coefficient of performance (COP) of the heat pump is dependent on the outside air temperature [14]. The power generation efficiency and the efficiency of thermal power for the SOFC are maintained at constant values and are related to the performance and cost of hydrogenation, dehydration, and water electrolysis [10]. The reason for having used the heat to power ratio of fixed SOFC is that analysis becomes easy. Table 3 presents information relating to the cost of the equipment. Furthermore, values of Table 3 were surmised from present product price. Wind power generation assumes a capacity of 2400 kW, while the large-scale solar power system assumes that bifacial solar cells are used [12]. The cost of the solar and wind power generation equipment is considered in conjunction with maintenance costs obtained from records of previous operations.

5.3 Analysis Method

Equations (10), (11), and (12) and (13) describe the electric power balance of the microgrid for the NAS battery, OCHM-A, and OCHM-B types of systems, respectively. Equation (14) is a heat balance equation common to all systems. The subscript $t$ indicates sampling time; the left-hand sides of Eq. (10) to Eq. (14) represent energy supply terms, while the right-hand sides represent energy consumption. The OCHM-B type is divided into a hydrogen generation system driven by renewable energy (Eq. (12)) and a power supply system that is linked to the distribution network and heat pump by SOFCs (Eq. (13)). Although $P_{GW}$ is the output of a wind power generator, the wind farm consists of a set of $N_{GW}$ generators, each with a maximum output of 2400 kW; these wind power generators are installed in areas where wind speed is high, i.e., the coastal area or the ridges of the mountains surrounding Kitami. Moreover, although $P_{GS}$ represents the output of one double-sided solar cell, the large-scale solar power system consists of a set of $N_{GS}$ systems. The value of $P_{GS}$ is calculated from the power generation area, power generation efficiency (Table 2), and slope face solar insolation at Kitami. $\Delta P_{need}$ on the right-hand side of Eqs. (10), (11), and (13) represents the power demand of Kitami, which is obtained from the electricity demand characteristics of average individual houses and

the number of such houses present. Loss of electric power $\Delta P_{loss}$ represents the total power loss related to the equipment listed in Table 2. $\Delta P_{hp}$ is a power consumption term for the heat pump. The COP of the heat pump can be obtained when the outside air temperature is introduced into Fig. 7. Then, $\Delta P_{hp}$ can be obtained by dividing the heat demand of the entire Kitami region by this COP.

The supply and demand balance of electric power for the NAS battery system (Eq. (10)) is adjusted by varying the charge and discharge of $P_{NAS}$, i.e., the power of the NAS battery. The power consumption terms $P_{WE}$ and $P_{HC}$ are included in Eqs. (11) and (12) to represent the water electrolyzer and hydrogen compressor, respectively, in the OCHM systems. $P_{WE}$ is calculated from the efficiency of the water electrolyzer (Table 2) and the amount of power supplied, while $P_{HC}$ is obtained from Eq. (9). When the electricity supplied by renewable energy exceeds the demand (excluding that of the water electrolyzer and hydrogen compressor), as defined by the right hand-side of Eq. (11), the surplus power is supplied to the water electrolyzer and hydrogen is produced in the OCHM-A system. Then, methylcyclohexane is produced from toluene by supplying this hydrogen to the hydrogenation reactor, and the methylcyclohexane produced is stored in a pressure tank. When the power supply generated from renewable energy is insufficient to meet the power demands, as defined by the right-hand side of Eq. (11), the SOFC is operated using hydrogen obtained by dehydration of stored methylcyclohexane. All electric power derived from renewable energy ($P_{GW}$ and $P_{GS}$) is given to the water electrolyzer and hydrogen compressor in the OCHM-B system (Eq. (12)), and methylcyclohexane is produced by hydrogen through water electrolysis and the hydrogenation of toluene. Hydrogen can subsequently be produced by supplying this methylcyclohexane to the dehydration reactor installed near the SOFC, supplying hydrogen to the SOFC to provide electric power at the demand side (Eq. (13)).

The amount of renewable energy introduced into each type of microgrid is set as a parameter and the capacity of the energy storage equipment (NAS battery, water electrolyzer, and so on) is decided by the annual energy balance. The cost of each type of microgrid depends primarily on the unit price of equipment (Table 3) and equipment capacity.

Power balance of the NAS battery system

$$\sum_{l=1}^{N_{GW}} P_{GW,l,t} + \sum_{m=1}^{N_{GS}} P_{GS,m,t} + P_{NAS,t} = \sum_{n=1}^{N_{need}} \Delta P_{need,n,t} + \sum_{o=1}^{N_{hp}} \Delta P_{hp,o,t} + \sum_{p=1}^{N_{loss}} \Delta P_{loss,p,t} \tag{10}$$

Power balance of the OCHM-A system

$$\begin{aligned} &\sum_{l=1}^{N_{GW}} P_{GW,l,t} + \sum_{m=1}^{N_{GS}} P_{GS,m,t} + \sum_{q=1}^{N_{SOFC}} P_{SOFC,q,t} \\ &= \sum_{n=1}^{N_{need}} \Delta P_{need,n,t} + \sum_{o=1}^{N_{hp}} \Delta P_{hp,o,t} + \sum_{r=1}^{N_{WE}} \Delta P_{WE,r,t} + \sum_{s=1}^{N_{HC}} \Delta P_{HC,s,t} + \sum_{p=1}^{N_{loss}} \Delta P_{loss,p,t} \end{aligned} \tag{11}$$

Power balance of the OCHM-B system

$$\sum_{l=1}^{N_{GW}} P_{GW,l,t} + \sum_{m=1}^{N_{GS}} P_{GS,m,t} = \sum_{r=1}^{N_{WE}} \Delta P_{WE,r,t} + \sum_{s=1}^{N_{HC}} \Delta P_{HC,s,t} + \sum_{p=1}^{N_{loss}} \Delta P_{loss,p,t} \tag{12}$$

$$\sum_{q=1}^{N_{SOFC}} P_{SOFC,q,t} = \sum_{n=1}^{N_{need}} \Delta P_{need,n,t} + \sum_{o=1}^{N_{hp}} \Delta P_{hp,o,t} + \sum_{p=1}^{N_{loss}} \Delta P_{loss,p,t} \quad (13)$$

Heat balance of all types of microgrid

$$\sum_{o=1}^{N_{hp}} H_{hp,o,t} = \sum_{n=1}^{N_{need}} \Delta H_{need,n} + \Delta H_{loss,t} \quad (14)$$

## 6. Results and Discussion

### 6.1 Operational Results for the NAS Battery

Figure 8 illustrates the results of the operational analysis of the microgrid incorporating a NAS battery. Figure 8 (a) presents the power consumption (right-hand side of Eq. (10)) for a representative day and the monthly electricity supply derived from renewable sources, while Fig. 8 (b) presents the operational results for the NAS battery. The capacity of the NAS battery is set to balance the annual supply and demand of the system, as described by Eq. (10). In addition, much charging (discharging) occurs from March to November (December to February) owing to the power consumption of the heat pump.

### 6.2 Installed Capacity of the OCHM Type Microgrid

Figures 9 (a) and (b) illustrate the supply capability (including that of the wind farm, large-scale solar power system, and SOFC) of the microgrid for the OCHM-A and OCHM-B systems and the power consumed by the heat pump. The labels A1–A9 represent combinations of the power generation area of bifacial solar cells and the number of 2400-kW wind power generators installed. To satisfy the energy balance equations (Eqs. (11–14)), the power generated by photovoltaics will increase as that generated by wind power decreases. However, possible increases in the capacity of photovoltaics are small compared to the possible reduction of wind power generation, as shown in Figs. 9 (a) and (b). Moreover, wind speed is low in the region where the wind farm is located, meaning that production of electricity does not increase with increasing capacity for wind power generation. Therefore, the introductory capacity of the SOFC is not related to the amount of renewable energy introduced from both sources.

### 6.3 Equipment Cost

The cost of each microgrid investigated in this study represents the sum total of equipment and maintenance costs for a 20-year period. The results of the cost analysis for all types of microgrids are shown in Fig. 10. However, the facilities cost for the power transmission and distribution lines were not included in the microgrids. Moreover, the cost of land transportation was not considered for the OCHM-B system.

The combinations of renewable energy types (A1–A9) shown in Figs. 10 (b) and (c) for the OCHM system represent the same as those illustrated in Figs. 9 (a) and (b), respectively. Similarly, the combinations for the NAS battery system (A1 to A7) are shown in Fig. 10 (a). A reduction in the amount

of wind power generated results in a lower facilities cost, which decreases as more photovoltaics are introduced in the cost analysis for the NAS battery system (Fig. 10 (a)). Wind conditions are poor at the introductory point of the wind farm, and There are more annual productions of electricity of large-scale solar power systems than wind farm. The relationship between the energy combination and the facilities cost exhibits a similar trend for both the OCHM and NAS battery systems.

Figures 10 (b) and (c) present the facilities cost of the microgrid for the OCHM-A and OCHM-B systems, respectively. For the microgrid of the OCHM-A system, equipment cost comprises 74% of the total cost, with maintenance and personnel costs comprising the remainder. Similarly, equipment cost represents 79% of the facilities cost for the OCHM-B system. The equipment cost for hydrogenation and dehydration and the cost of the water electrolyzer are comparatively small. Energy combination A5 represents the minimum cost option for the microgrid of the OCHM-A system, while option A6 represents the minimum cost for the OCHM-B system. Moreover, with energy combination A5 for OCHM-A, the cost of the system is 12% lesser than that with energy combination A6 for OCHM-B. The cost of the microgrid of the OCHM-A system is advantageous to the OCHM-B system. This reason is because there are many losses in hydrogen production and energy storage by organic hydride. Furthermore, the OCHM-A system has few quantities to be stored of organic hydride to the OCHM-B system. The efficiencies of dehydration of the OCHM and hydrogen production are 85% and 71%, respectively, as shown in Table 2. Therefore, the installed capacity of renewable energy and the equipment costs of the entire system will be increased when large amounts of energy are stored using the OCHM. Moreover, the exhaust heat of the SOFC can be considered part of the heat demand for the microgrid of the OCHM-A system.

Figure 11 illustrates the results of cost analysis for a 20-year period for both the NAS battery and OCHM systems. The NAS battery system costs less than the OCHM systems for the conditions analyzed in the present study. Therefore, an energy storage system incorporating the OCHM can be considered economically disadvantageous. The minimum equipment cost of the NAS battery system is 16% cheaper than that of the OCHM-A system. The microgrid with energy storage by organic hydride produces large loss by the water electrolyzer and the dehydratio reactor. Therefore, the renewable energy of OCHM-A system is large scale compared with the NAS battery system. Therefore, improvements in the efficiency of the water electrolyzer and dehydration reactor must be achieved for implementation of a microgrid of OCHM system.

### 6.4 Operational Results for OCHM Systems

Figure 12 illustrates the results of operational analysis of a representative day for each month in order to assess minimum equipment cost (A5 and A6 in Figs. 9 (a) and 9 (b), respectively) for the OCHM-A and OCHM-B systems. Because wind velocity is high along the coast of Kitami in November, the wind farm can produce considerable amounts of electricity at this time (Figs. 12 (a) and (b)). The amount of energy stored by a hydrogen medium incorporating OCHM is greater for the OCHM-B system for all months. When the electricity generated by renewable energy is insufficient to meet the energy demand, electricity is supplied to the demand side from the SOFC in the microgrid of the

OCHM-A system. Therefore, the capacity of the SOFC installed in the microgrid of the OCHM-A system is expected to be smaller than that of the OCHM-B system and is usually generated according to the load. However, the operating pattern of the SOFC in Figs. 12 (a) and (b) barely changed so that there is little difference in the capacity of the SOFC between the OCHM-A and OCHM-B systems.

## 7. Conclusions

Change in the output of renewable energy considerably influences the quality of electric power in independent microgrids designed to realize local supply and consumption of energy. Accordingly, operating methods and costs were analyzed for a microgrid incorporating two types of energy storage equipment: a sodium–sulfur (NAS) battery, and a hydrogen medium incorporating the organic chemical hydride methylcyclohexane (OCHM). The installed capacity and cost were clarified, assuming the introduction of an independent microgrid in Kitami City, a cold region in Japan. The OCHM-A system was designed to simulate energy storage similar to that of a battery, while OCHM-B was simulated to substitute power transmission or transportation of the OCHM. The conclusions of the investigation can be summarized as follows.

(1) The facilities cost of the microgrid decreased with reduction of the amount of wind power generated and a concomitant increase in the amount of photovoltaics introduced. For this reason, storage capacity is determined according to the maximum output of the wind farm. Furthermore, wind conditions at the introductory point were found to be poor, suggesting that the annual production of electricity by the large-scale solar power system should be large.

(2) Equipment costs for the OCHM-A and OCHM-B systems represented 74% and 79% of their respective facilities costs (where the cost of the electrical power grid is not included). The costs of the water electrolyzer, hydrogenation reactor, and dehydration reactors are extremely small relative to the cost of generating the energy. In addition, the microgrid for the OCHM-A system was found to be 12% cheaper than that for the OCHM-B system.

(3) Because energy storage by the OCHM is inefficient owing to the inefficiency of the water electrolyzer and dehydration reactor, an OCHM system requires renewable energy to be produced on a much larger scale compared with a NAS battery system. Therefore, the cost of the system tends to increase with reduction in the installed capacity required to make the OCHM system viable. Improvements in the efficiency of the water electrolyzer and dehydration reactor are important for realization of OCHM-type microgrids.

(4) The capacity of the SOFC introduced into the microgrids of the OCHM-A and OCHM-B systems is unrelated to the energy combination adopted.

Nomenclature

| | | |
|---|---|---|
| AC | : | Alternating current |
| $C_{Comp,H_2}$ | : | Compression pressure of hydrogen [MPa] |
| $C_{\infty}$ | : | Atmospheric pressure [MPa] |
| DC | : | Direct current |

| | | |
|---|---|---|
| DH | : | Dehydrogenation equipment |
| $H$ | : | Heat [kWh] |
| $\Delta H$ | : | Consumption of heat power [kW] |
| $I$ | : | Current [A] |
| $K_{c,t}$ | : | Temperature coefficient |
| $L_{c,H_2}$ | : | Work of hydrogen compressor [Nm] |
| $N$ | : | Number |
| NAS | : | Sodium–sulfur battery |
| $n$ | : | Number of revolutions of power generator [rpm] |
| $n_o$ | : | Synchronous speed [rpm] |
| OCHM | : | Organic chemical hydride |
| $P$ | : | Effective electric power [kW] |
| $\Delta P$ | : | Consumption of electric power [kW] |
| $P_s$ | : | Signal of pressure gauge |
| PWM | : | Pulse width modulation |
| $Q$ | : | Reactive power [var] |
| $s$ | : | Sliding |
| SC | : | Bus line |
| SOFC | : | Solid oxide fuel cell |
| $T$ | : | Temperature [K] |
| $t$ | : | Sampling time [h] |
| $U_\infty$ | : | Flow of hydrogen [$m^3/s$] |
| $V$ | : | Voltage [V] |

Greek characters

| | | |
|---|---|---|
| $\varphi_c$ | : | Overall efficiency of compressor |

Subscript

| | | |
|---|---|---|
| fc | : | Fuel cell |
| *GS* | : | Photovoltaics |
| *GW* | : | Wind power generator |
| *HC* | : | Hydrogen compressor |
| *hp* | : | Heat pump |
| *loss* | : | Loss |
| *need* | : | Demand |
| pv | : | Photovoltaics |
| *WE* | : | Water electrolysis |
| wp | : | Wind power generation |

## References

[1] June K M, Chang H L. Numerical study on the thermal management system of a molten

sodium-sulfur battery module. J Power Sources 2012;210:101–109.
[2] Zhaoyin W, Jiadi C, Zhonghua G, Xiaohe X, Fuli Z, Zuxiang L. Research on sodium sulfur battery for energy storage. Solid State Ionics 2008;179:1697–1701.
[3] Cheol W P, Ho S R, Ki W K, Jou H A, Jai Y L, Hyo J A. Discharge properties of all-solid sodium–sulfur battery using poly (ethylene oxide) electrolyte. J Power Sources 2007;165:450–454.
[4] Sone A, Kato T, Shimakage T, Suzuoki Y. Influence of forecast accuracy of photovoltaic power output on capacity optimization of microgrid composition under 30-minute power balancing control. Electrical Engineering in Japan 2013;182:20–29.
[5] Carl J R, Björn A S. Energy analysis of batteries in photovoltaic systems. Part I: Performance and energy requirements. Energ Convers Manage 2005;46:1957–1979.
[6] Okada Y, Sasaki E, Watanabe E, Hyodo S, Nishijima H. Development of dehydrogenation ca
talyst for hydrogen generation in organic chemical hydride method. Int J Hydrogen Energy 2006; 31:1348-1356.
[7] Rajesh B B, Rayalu S, Devotta S, Ichikawa M. Chemical hydrides: A solution to high capacity hydrogen storage and supply. Int J Hydrogen Energy 2008;33:360–365.
[8] Anshu S, Shilpi K, Rajesh B B. Hydrogen delivery through liquid organic hydrides: Considerations for a potential technology. Int J Hydrogen Energy 2012;37:3719–3726.
[9] NGK Insulators, LTD., http://www.ngk.co.jp/english/products/power/nas/index.html, 2012
[10] Hrein Energy Inc., http://www.hrein.jp/english/index.htm, 2012.
[11] Section 5.3 Introductory concept for hydrogen supply base by green energy, Kumejima-cho new energy vision, Kumejima town office, http://www.town.kumejima.okinawa.jp/industry/new_enevision.html, 2013. In Japanese
[12] PVG solutions Inc., http://www.pvgs.jp/files/ja/PVGS_Catalogue_Oct2011.pdf, 2013.
[13] Japanese Meteorological Agency, http://www.jma.go.jp/jma/index.html, 2013
[14] The development of the $CO_2$ heat pump hot water supply unit for business use that can be operated down to -25 degrees Celsius of outside air temperature, Technical report of Mitsubishi heavy industries, LTD., 2011;48(4):86–88.

Captions

Fig. 1 Independent microgrid with NAS battery or OCHM system
(a) NAS battery type
(b) OCHM-A type
(c) OCHM-B type

Fig. 2 Block diagram of proposed system
(a) NAS battery type
(b) OCHM type

Fig. 3 NAS battery
(a) Schematic of the cell stack of a NAS battery
(b) Block diagram of a NAS battery
(c) Characteristics of temperature dependence of the battery (battery cell stack)

Fig. 4 Hydrogenation system
(a) Configuration of the hydrogenation system
(b) Characteristics of temperature dependence of the water electrolyzer and hydrogenation reactor

Fig. 5 Dehydrogenation system
(a) Configuration of the dehydrogenation system
(b) Characteristics of temperature dependence of dehydrogenation

Fig. 6 Kitami City microgrid

Fig. 7 Performance of the heat pump

Fig. 8 Operational analysis results for the NAS battery system
(a) Analysis results for electric power supply and demand
(b) Operational analysis results for charge and discharge of the NAS battery

Fig. 9 Capacity analysis results for the OCHM-type system
(a) OCHM-A system
(b) OCHM-B system

Fig. 10 Cost analysis results for each system for a 20-year period
(a) NAS battery system
(b) OCHM-A system
(c) OCHM-B system

Fig. 11 Analysis results for operation and equipment cost for a 20-year period

Fig. 12 Operational analysis results for the OCHM-type system
(a) OCHM-A system for A5
(b) OCHM-B system for A6

Table 1 Specifications of NAS battery and OCHM

Table 2 Performance of equipment

Table 3 Unit price for setup

Fig. 1　Independent microgrid with NAS battery or OCHM system

(a) NAS battery type

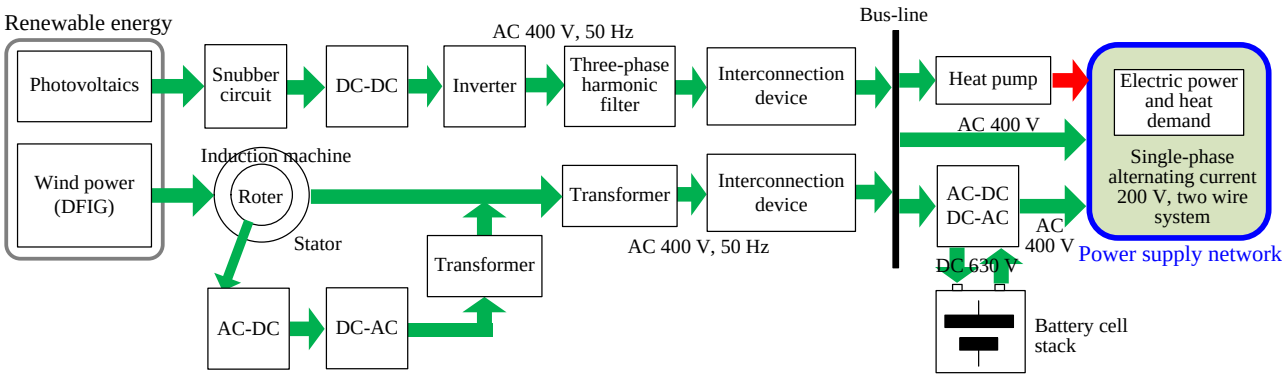

Fig. 1　Independent microgrid with NAS battery or OCHM system
(b) OCHM-A type

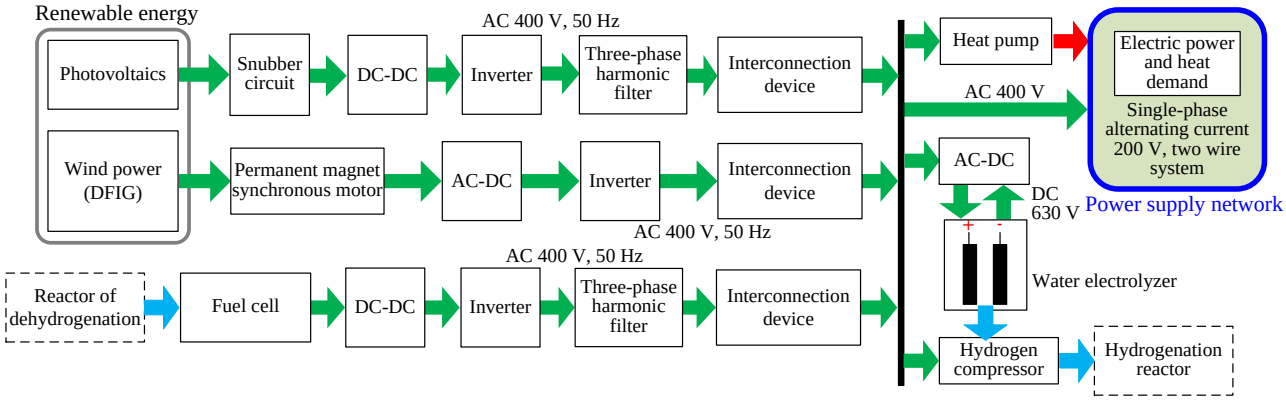

Fig. 1　Independent microgrid with NAS battery or OCHM system
(c) OCHM-B type

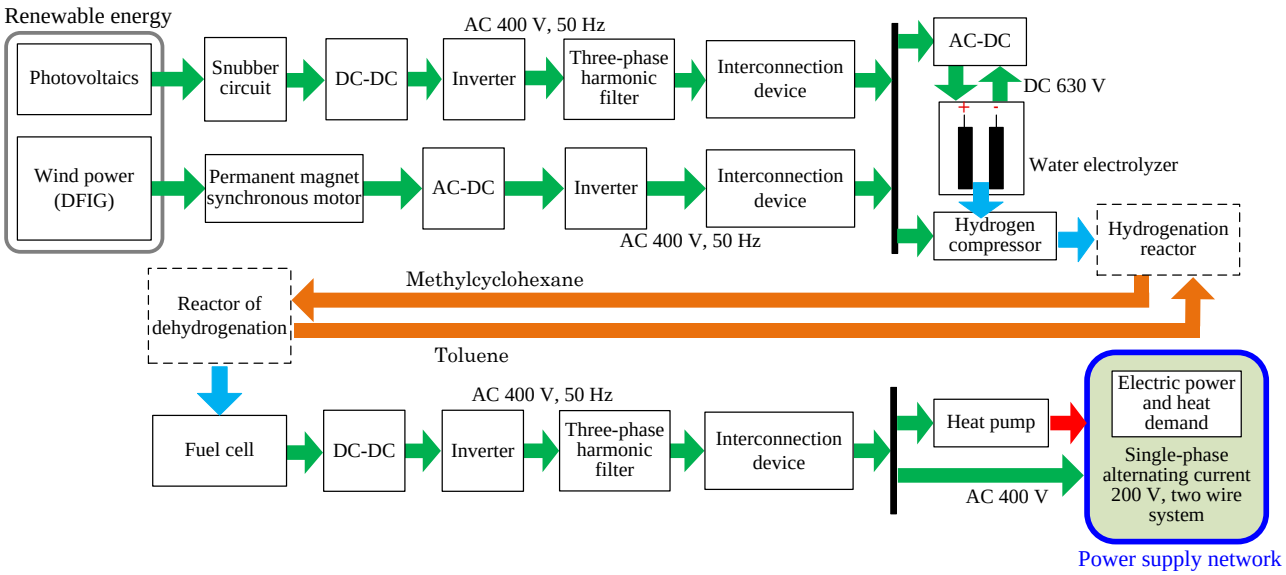

Fig. 2　Block diagram of the proposed system

(a) NAS battery type

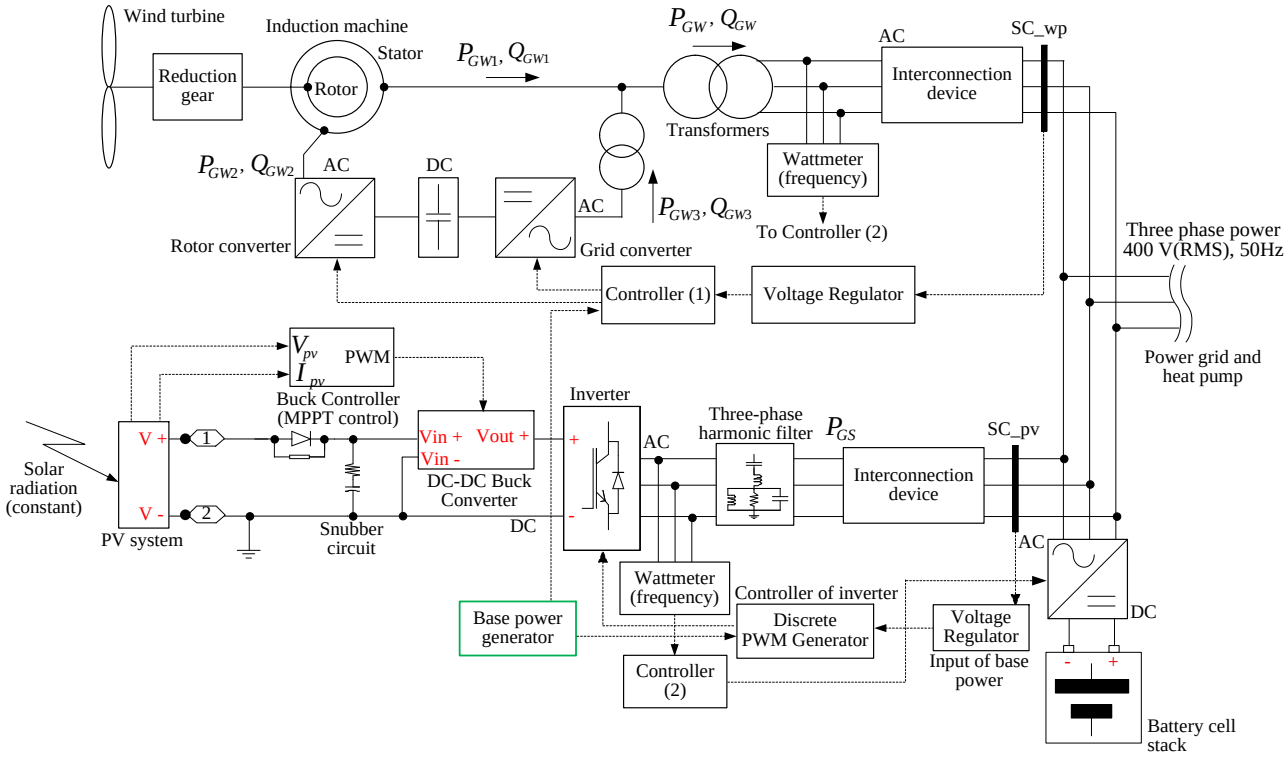

Fig. 2　Block diagram of the proposed system

(b) OCHM type

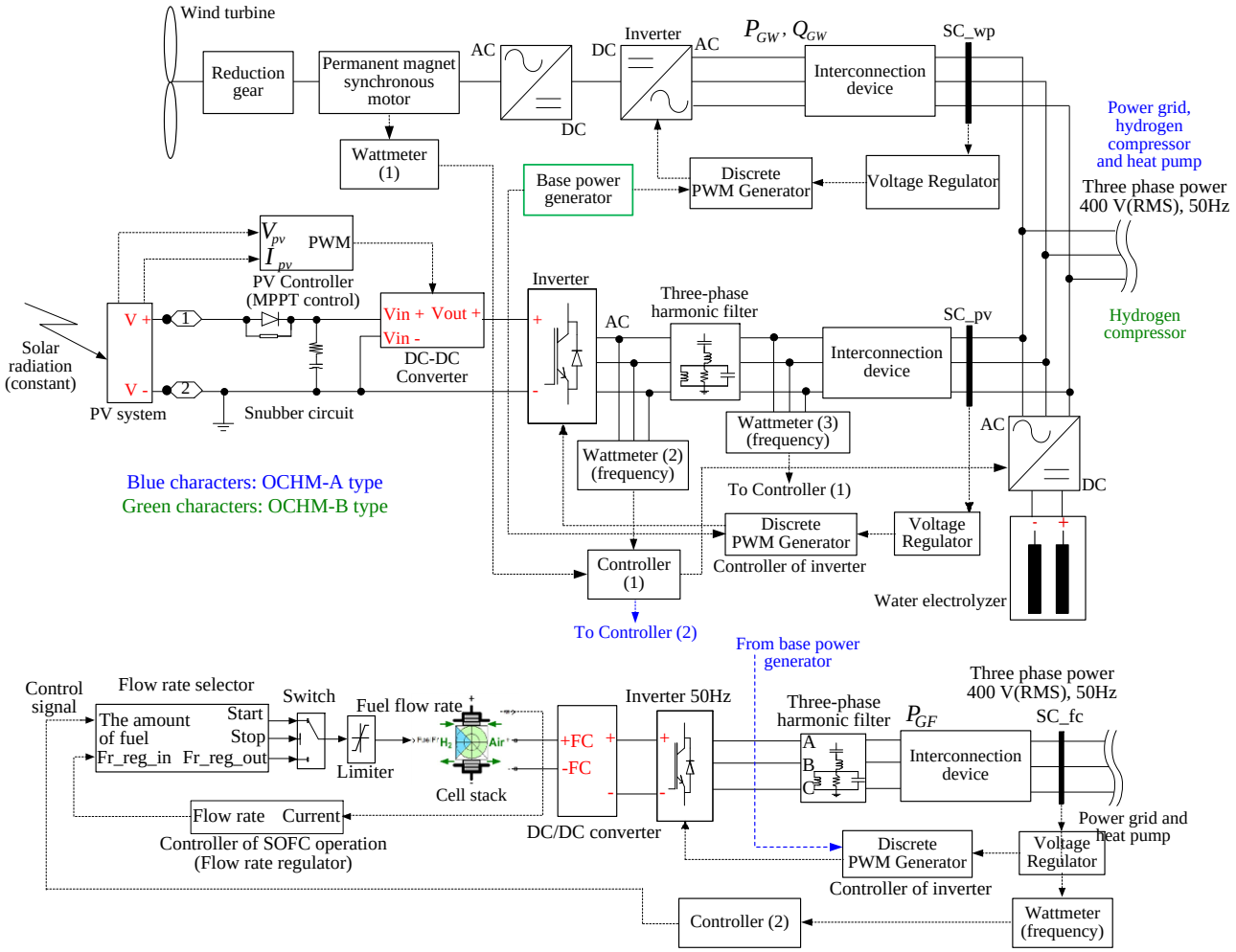

Fig. 3　NAS battery

(a) Schematic of a cell stack of a NAS battery

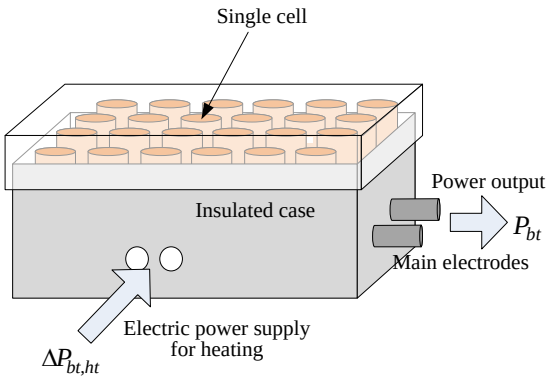


(a) Scheme of cell stack of NAS battery

Fig. 3　NAS battery

(b) Block diagram of a NAS battery

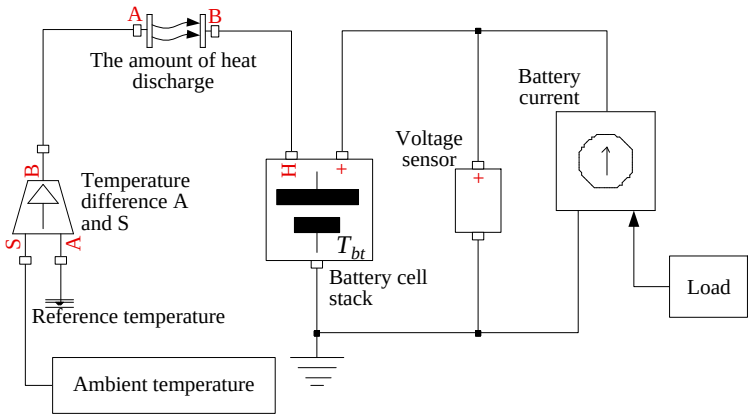

Fig. 3　NAS battery

(c) Characteristics of temperature dependence of the battery (battery sell stack)

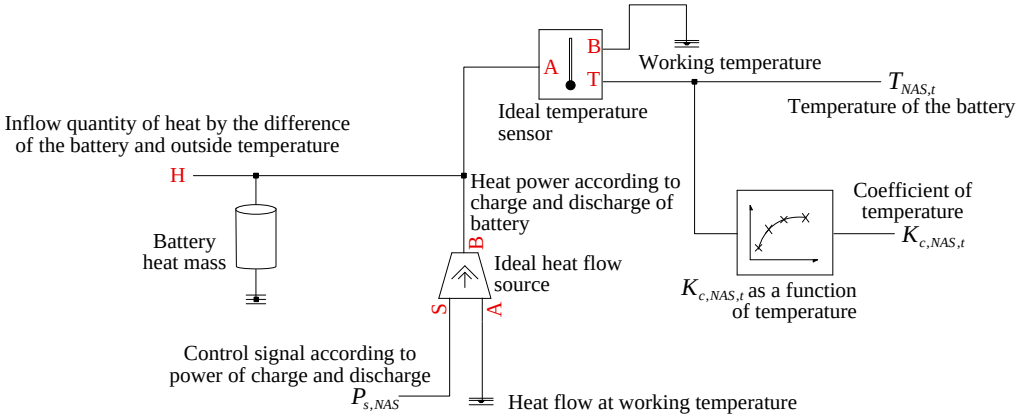

Fig. 4　Hydrogenation system

(a) Configuration of hydrogenation

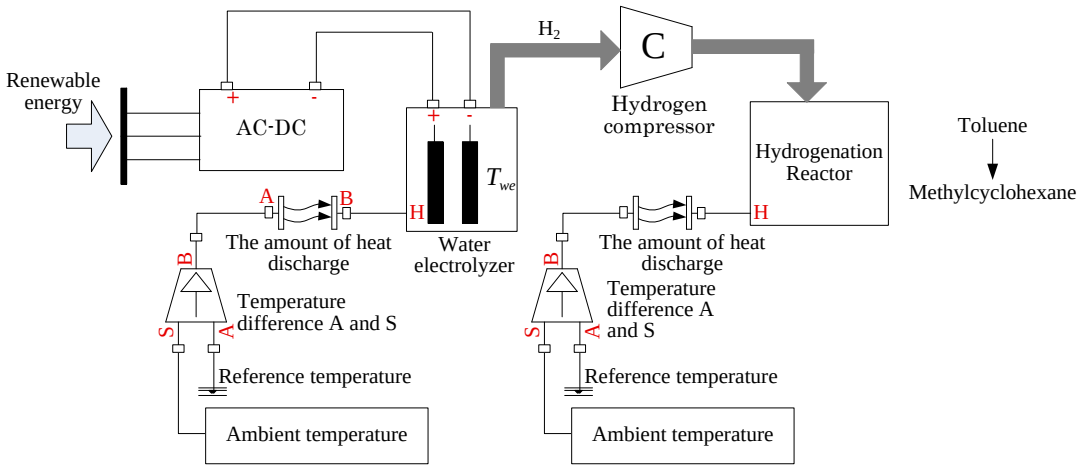

Fig. 4　Hydrogenation system

(b) Characteristics of temperature dependence of the water electrolyzer and hydrogenation reactor

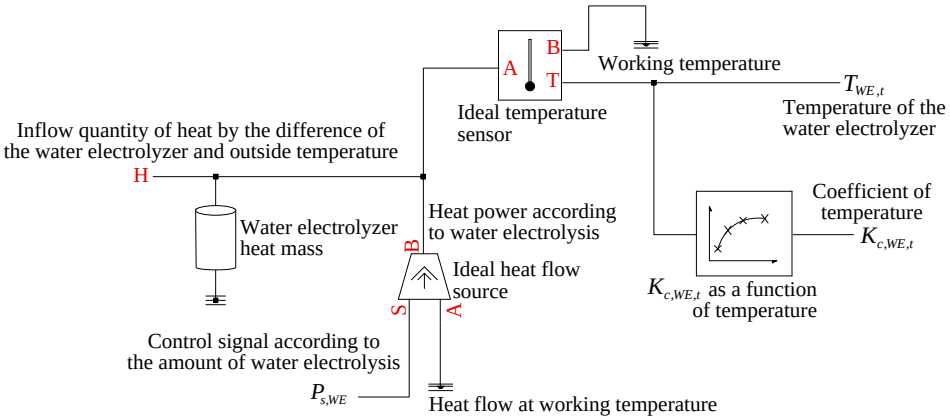

Fig. 5　Dehydrogenation system

(a) Configuration of the dehydrogenation system

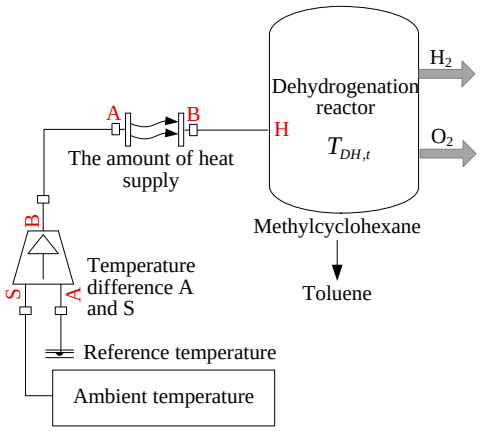

Fig. 5　Dehydrogenation system

(b) Characteristics of temperature dependence of dehydrogenation

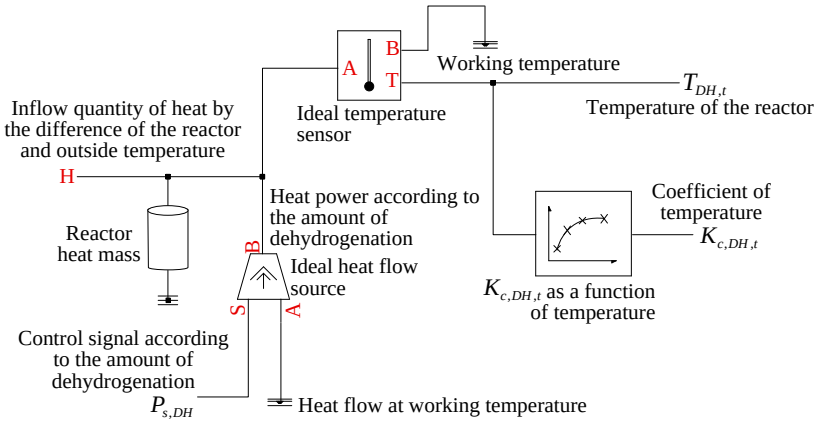

Fig. 6　Kitami city microgrid

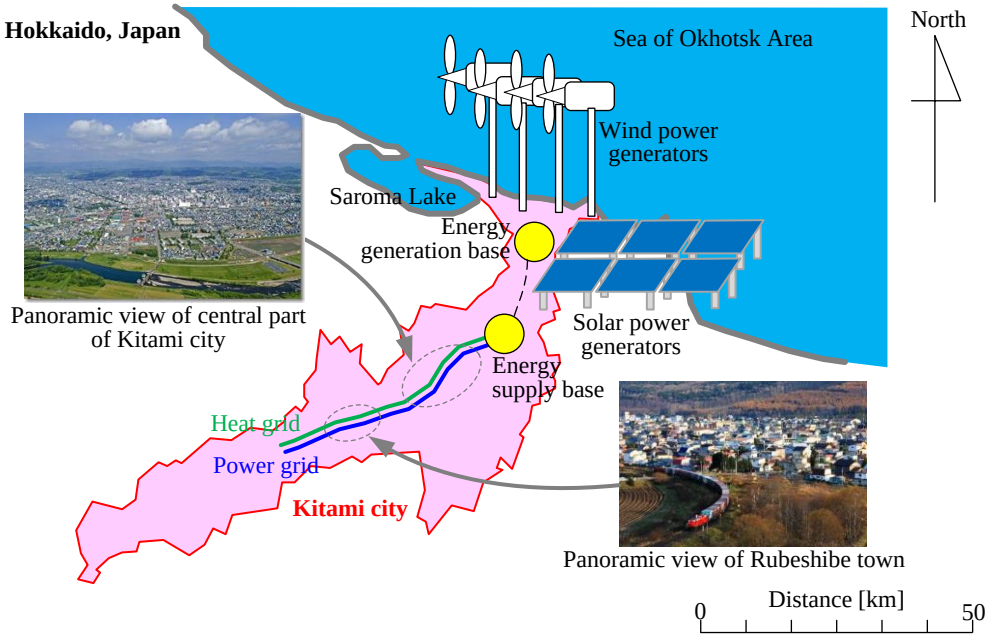

Fig. 7　Performance of the heat pump

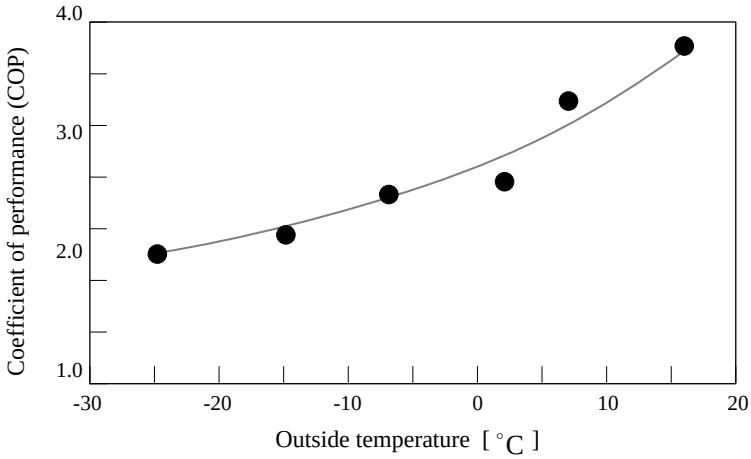

Fig. 8 Operational analysis results for the NAS battery system

(a) Analysis results for electric power supply and demand

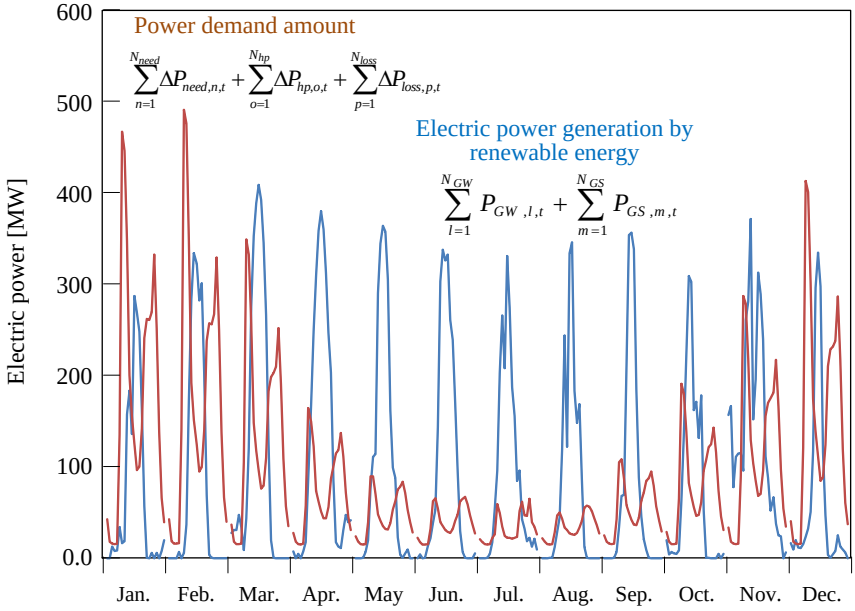

Fig. 8　Operational analysis results for the NAS battery system

(b) Operational analysis results for charge and discharge of the NAS battery

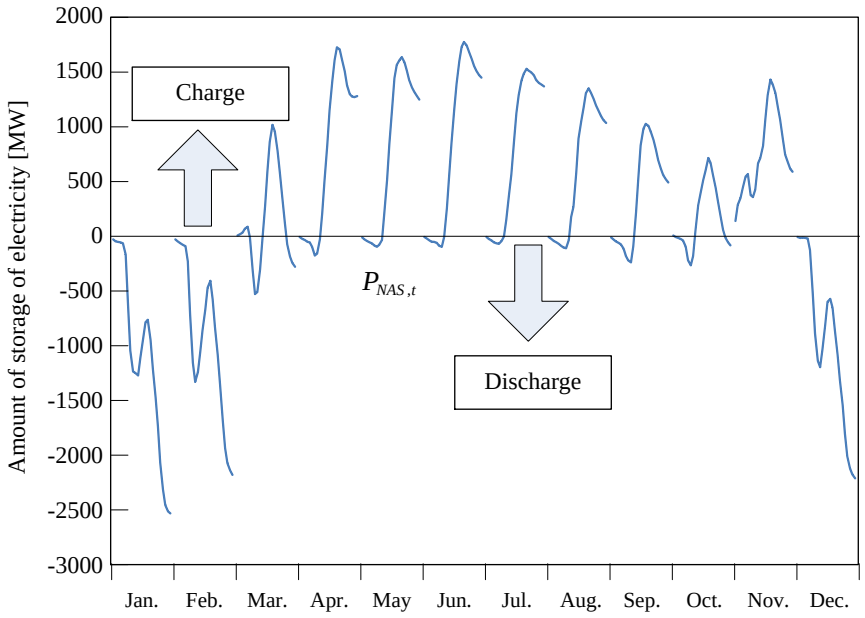

Fig. 9　Capacity analysis results for the OCHM systems

(a) OCHM-A system

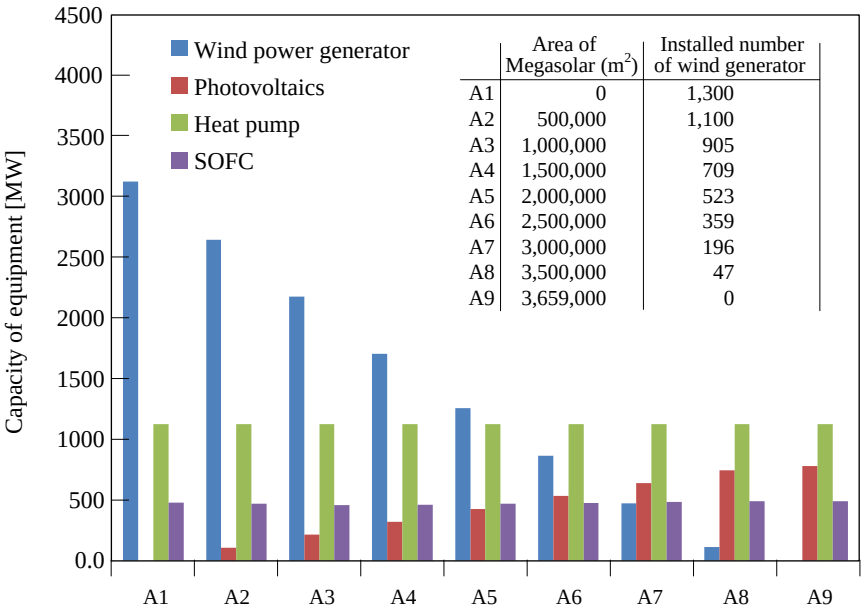


| | Area of Megasolar ($m^2$) | Installed number of wind generator |
|---|---|---|
| A1 | 0 | 1,300 |
| A2 | 500,000 | 1,100 |
| A3 | 1,000,000 | 905 |
| A4 | 1,500,000 | 709 |
| A5 | 2,000,000 | 523 |
| A6 | 2,500,000 | 359 |
| A7 | 3,000,000 | 196 |
| A8 | 3,500,000 | 47 |
| A9 | 3,659,000 | 0 |

Fig. 9　Capacity analysis results for the OCHM systems

(b) OCHM-B system

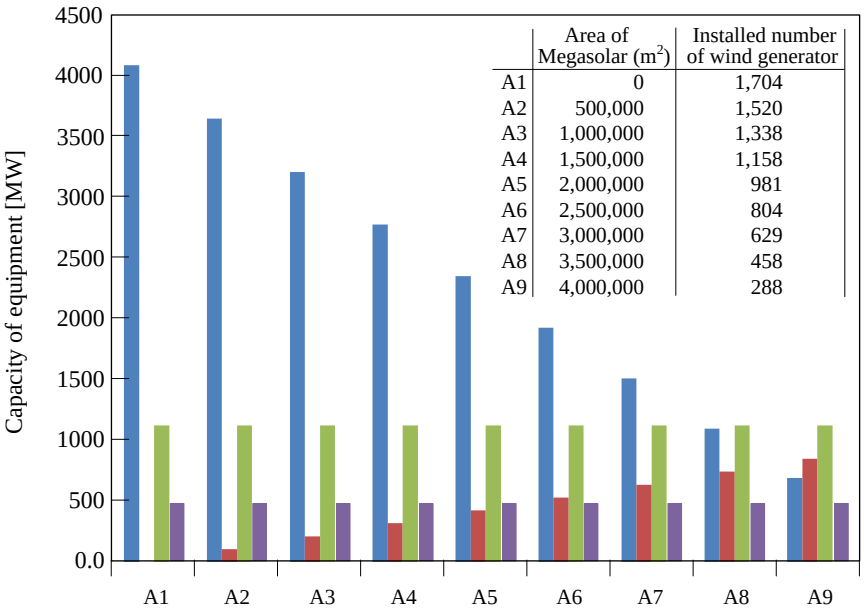


| | Area of Megasolar ($m^2$) | Installed number of wind generator |
|---|---|---|
| A1 | 0 | 1,704 |
| A2 | 500,000 | 1,520 |
| A3 | 1,000,000 | 1,338 |
| A4 | 1,500,000 | 1,158 |
| A5 | 2,000,000 | 981 |
| A6 | 2,500,000 | 804 |
| A7 | 3,000,000 | 629 |
| A8 | 3,500,000 | 458 |
| A9 | 4,000,000 | 288 |

Fig. 10　Cost analysis results for each system for a 20-year period

(a) NAS battery system

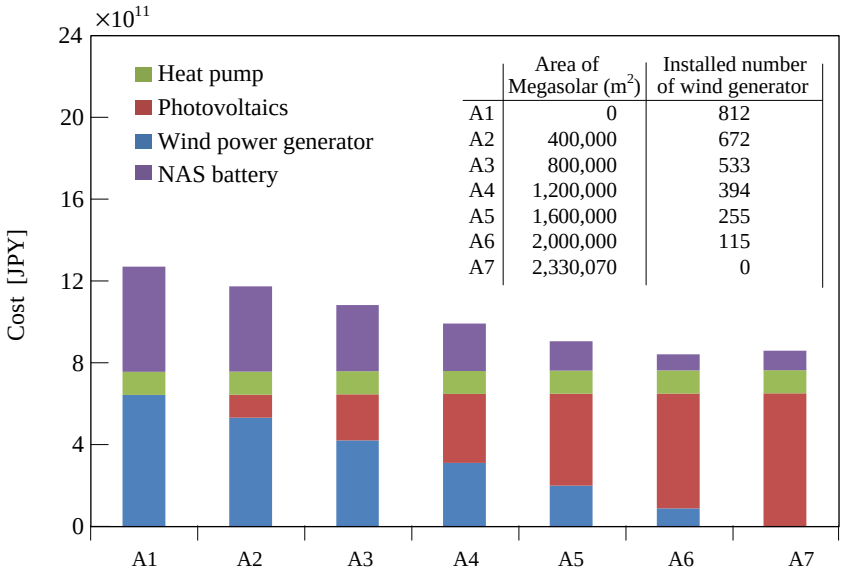


| | Area of Megasolar ($m^2$) | Installed number of wind generator |
|---|---|---|
| A1 | 0 | 812 |
| A2 | 400,000 | 672 |
| A3 | 800,000 | 533 |
| A4 | 1,200,000 | 394 |
| A5 | 1,600,000 | 255 |
| A6 | 2,000,000 | 115 |
| A7 | 2,330,070 | 0 |

Fig. 10　Cost analysis results for each system for a 20-year period
(b) OCHM-A system

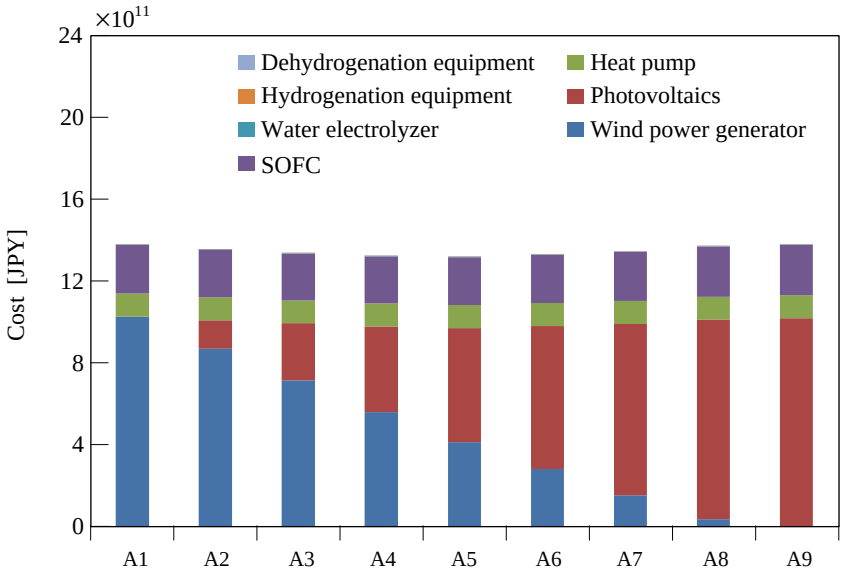

Fig. 10　Cost analysis results for each system for a 20-year period
(c) OCHM-B system

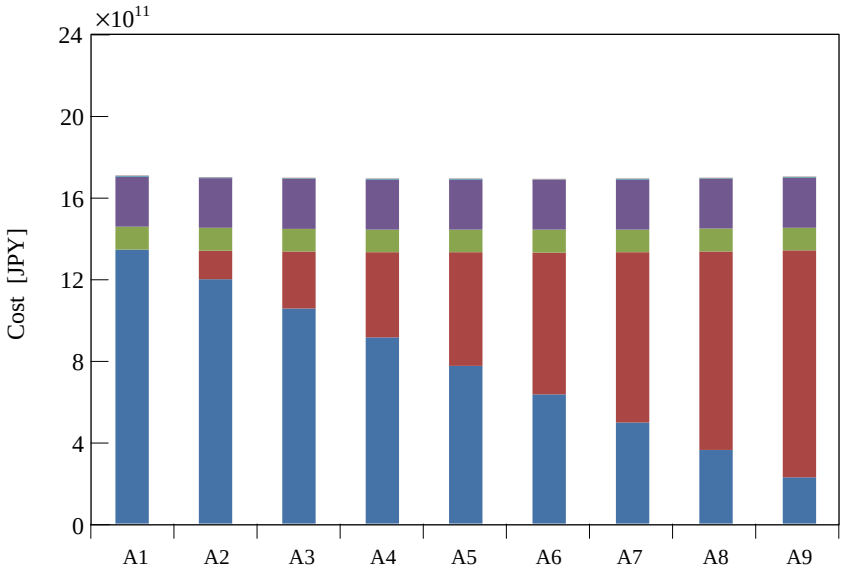

Fig. 11　Analysis results for operation and equipment cost for a 20-year period

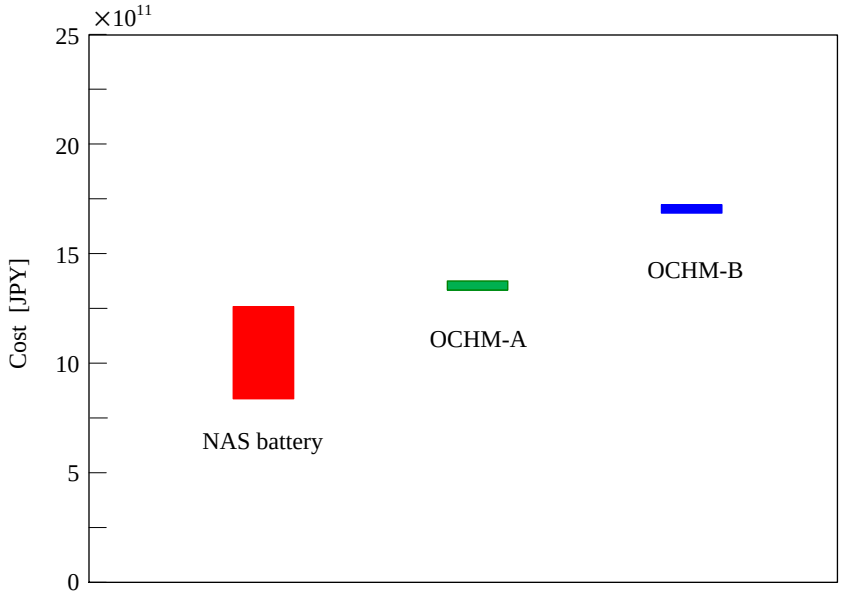

Fig. 12　Operational analysis results for the OCHM-type system
(a) OCHM-A system for A5

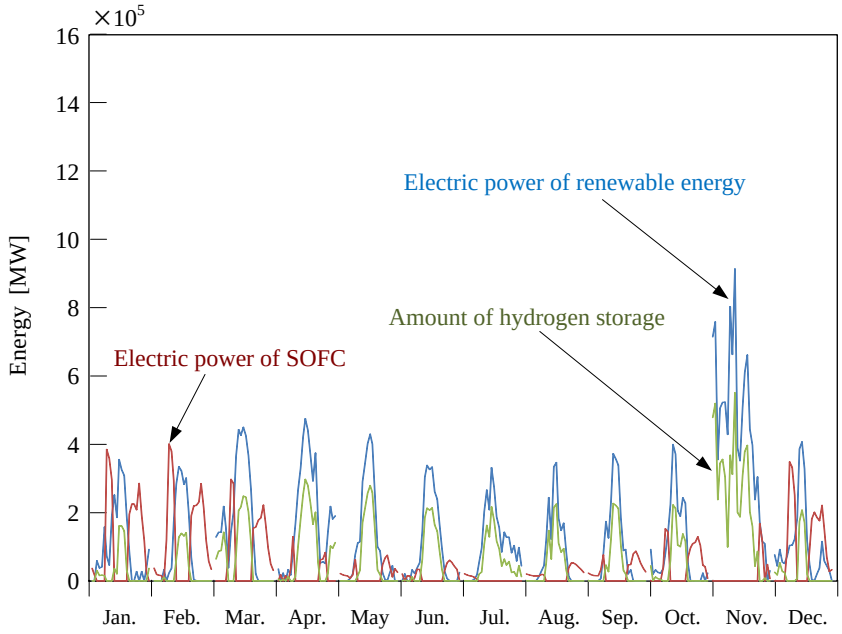

Fig. 12　Operational analysis results for the OCHM-type system
(b) OCHM-B system for A6

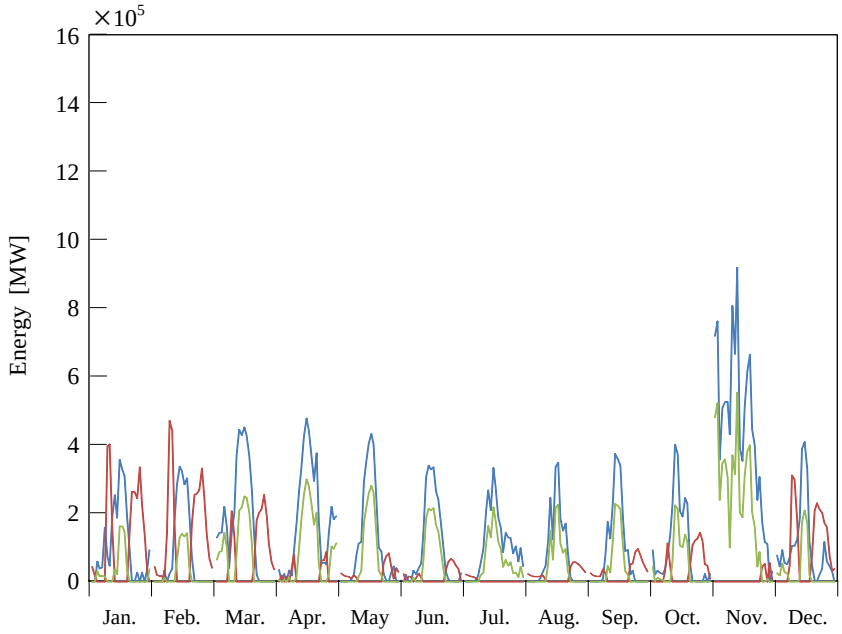

Table 1　Specifications of the NAS battery and OCHM

Japanese Yen（1 USD=94 JPY）

| | NAS battery | Organic chemical hydride (methylcyclohexane) |
|---|---|---|
| Energy density [Wh/kg] | 784(theoretical), 100-160(real) | 684 |
| Efficiency of discharge and charge [%] | 75 (AC) | 50 (Heating value of hydrogen) [*1] |
| Design life of equipment [Year] | 15 (4500 cycle) | - |
| Self-discharge [%/h] | None | None |
| Equipment cost [JPY/kWh] | 25,000 | 170,000 |
| Operation cost [JPY/kW] | 200,000 | 18.8 |
| Application scale [kW] | 2000 - tens of thousands | No limit |

[*1]12000 kg/day, Transportation distance of 50 km.

Table 2　Performance of equipment

| Equipment | Efficiency |
|---|---|
| Inverter | 0.95 |
| DC-DC converter | 0.97 |
| AC-DC converter | 0.97 |
| SOFC (electric power) | 0.5 |
| SOFC (heat) | 0.35 |
| COP of heat pump | Fig. 7 |
| Wind power generator | 0.335 |
| Photovoltaics (bifacial solar ell) | 0.213 |
| Temperature loss of solar cell | 0.4 %/K |
| Water electrolysis | 0.71 |
| Reactor of hydrogenation | 0.99 |
| Reactor of dehydrogenation | 0.85 |
| Charge-discharge efficiency of NAS | 0.75 |
| Hydrogen compressor | 0.5 |

Table 3　Unit price for the setup

Japanese yen（1 USD=94 JPY）

| | |
|---|---|
| Photovoltaics | 325,000 JPY/kW |
| Rental expense of land | 150 JPY/$m^2$ |
| Maintenance | 15 %/Year |
| Personnel expenses | 3,000,000 JPY/Year |
| Wind turbine | 210,000 JPY/kW |
| Maintenance | 6,000 JPY/kW |
| SOFC | 500,000 JPY/kW |
| Heat pump | 100,000 JPY/kW |
| NAS battery | 25,000 JPY/kW |
| Water electrolysis, hydrogenation, dehydrogenation equipment | 4820 JPY/($m^3$/h) |